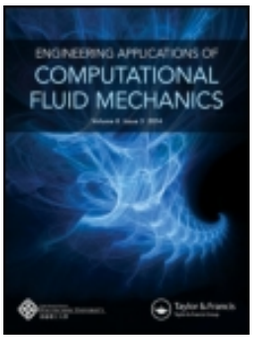

Engineering Applications of Computational Fluid Mechanics

ISSN: 1994-2060 (Print) 1997-003X (Online) Journal homepage: https://www.tandfonline.com/loi/tcfm20

Efficient methods for prediction of velocity fields in open channel junctions based on the artifical neural network

Amir Hossein Zaji & Hossein Bonakdari

To cite this article: Amir Hossein Zaji & Hossein Bonakdari (2015) Efficient methods for prediction of velocity fields in open channel junctions based on the artifical neural network, Engineering Applications of Computational Fluid Mechanics, 9:1, 220-232, DOI: 10.1080/19942060.2015.1004821

To link to this article: https://doi.org/10.1080/19942060.2015.1004821

Engineering Applications of Computational Fluid Mechanics, 2015
Vol. 9, No. 1, 220–232, http://dx.doi.org/10.1080/19942060.2015.1004821

Taylor & Francis
Taylor & Francis Group

Efficient methods for prediction of velocity fields in open channel junctions based on the artifical neural network

Amir Hossein Zaji and Hossein Bonakdari*

Department of Civil Engineering, Razi University, Kermanshah, Iran

(*Received 11 July 2014; final version received 3 September 2014*)

Measurement results, sediment transport and pollutant dispersion in confluence regions are highly affected by flow structures of open channel junction and it is necessary to find an efficient method that can fully describe the velocity fields in junctions. In this study the velocity field in an open channel junction was investigated by using Artificial Neural Network (ANN) and three dimensional modelling. First, a modified Genetic Algorithm (GA) was introduced, then, an ANN model was optimized and the flow velocity was predicted in a 90 degree channel junction. Also, for three dimensional simulation of the free surface flow in the considered junction ANSYS-CFX software was used. Comparison of the results obtained from ANN and CFX models with laboratory data with root mean square error of 0.094 and 0.182 and percent standard error of prediction of −9.75 and −25.71 respectively, showed that the introduced ANN perform better than CFX in modelling velocity field in open channel junction and it was able to predict accurate in different areas and flow-rates.

Keywords: open channel junction; artificial neural network; genetic algorithm; ANSYS-CFX; velocity fields

1. Introduction

Channel confluences are really significant in environmental and hydraulic engineering. Their flow structures highly affect measurement results, erosion, sediment transport and the dispersion of the pollutants in confluence regions. Open channel flow junctions, as considered in this paper, are those in which the flow from a lateral branch channel is entertained in a main channel.

In these flows, due to interaction between the main and branch flows, flow has a completely three dimensional behavior and calculating the characteristics of this complex flow requires precise and separate studies. The main flow features that characterize these configurations are zones of separation (or recirculation), the maximum and minimum velocity regions and a shear plane which is developed between the two joining flows downstream of the confluent channel. Numerous laboratory and theoretical analysis have been done to analyze and predict the characteristics of these flows (Taylor, 1944; Webber & Greated, 1966; Lin & Soong, 1979; Best & Reid, 1984; Ramamurthy, Carballada, & Tran, 1988; Biron, Best, & Roy, 1996; Wilcox, 1998; Chung-Chieh, Wen-Jung, & Cheng-Hsi, 1998). Conducting a laboratory study on the flow profile in a 90° channel junction, Weber, Schumate, and Mawer (2001) attempted to measure the velocity and depth in different flows and provide comprehensive information about the characteristics of flow in junctions. This extensive measurement provided an outstanding experimental data for validation.

For several decades experimental studies and theoretical analysis of flow junctions have been a great concern for engineers; however, three dimensional numerical modelling that employs computational fluid dynamic softwares is a recent phenomenon. Bradbrook, Biron, Lane, Richards, and Roy (1998), Bradbrook, Lane, and Richards (2000a), Bradbrook, Lane, Richards, Biron, and Ag (2000b) validated the application of three dimensional numerical model to simulate the flow structures in an open channel junction. Comparing the results obtained from their experiments Wang and Cheng (2000) investigated the performance of the three dimensional numerical model for the prediction of three dimensional side-discharge flows. Huang, Weber, and Lai (2002) used a three dimensional model and k-ω turbulence model to investigate the open channel junction flow and analyzed the effect of junction flow on flow characteristics. Shamloo and Pirzadeh (2008) used 2D numerical model to predict the velocity fields and dimension of separation zone in a T junction. Zhao, Zhu, and Rajaratnam (2008) established a computational fluid dynamics model to simulate fully surcharged flow at a 90 degree combining sewer junction. Shakibainia, Tabatabai, and Zarrati (2010) used a three dimensional numerical model, SSIIM2.0, and k-ω turbulence model to investigate the flow characteristics at separation zones, secondary currents, velocity profiles, and flow surface mapping indifferent confluence angles and discharge, ratios. Bonakdari, Lipeme-Kouyi, and Wang (2011) using a three dimensional

*Corresponding author. Email: bonakdari@yahoo.com

computational fluid dynamics model, analyzed the effect of discharge ratio on recirculation size and presented formulas to calculate the length and width of the separation zone in terms of discharge ratio for a 30° junction. Considering the distance from the junction, Dursun, Kaya, and Firat (2012) used 3D numerical model to analyze the junction's impact on the velocity fields to evaluate the error that is derived from calculating the flow rate close to the junction.

Due to the high capacity of soft computing method to analyze complex problems, this method has been used extensively in various hydraulic engineering problems such as discharge capacity of lateral weirs (Neary, & Sotiropoulos, 1996; Bilhan, Emiroglu, & Kisi, 2011), scour depth prediction (Muzzammil, 2010), flow characteristics in different open channels (Donmez, 2001; Grace & Priest, 1958; More, 1978), rainfall modeling and stream flow prediction (Asadi, Shahrabi, Abbaszadeh, & Tabanmehr, 2013; Chau, Wu, & Li, 2005; Chen & Chau, 2006; Cheng, Lin, Sun, & Chau, 2005; Firat & Gungor, 2008; Wu, Chau, & Li, 2009; Yurtseven, & Zengin, 2013), modelling coastal algal blooms (Muttil & Chau, 2006), evapotranspiration (Cobaner, 2011; Kisi, & Ozturk, 2007), combined open channel flow (Hager, 1987), sediment transport (Ebtehaj, & Bonakdari, 2013; Van Maanen, Coco, Bryan, & Ruessink, 2010), ground water level prediction (Taormina, Chau, & Sethi, 2012) and water demand forecasting (Pulido-Calvo & Gutierrez-Estrada, 2009; Tiwari, & Adamowski, 2013).

Artificial Neural Network (ANN) is one of the most applied methods for soft computing while it has comes in various types, with the simplest one being the Multi-Layer Perceptron (MLP). The present study was aimed to analyze the longitudinal velocity profile of flow in open channel junction and to measure its predictability by ANN and CFD models. To this end, the structure of a Levenberg-Marquardt ANN model was optimized by a new adaptive genetic algorithm. Also, a numerical model was made by ANSYS-CFX software for junctions' flow modeling. The accuracy of both ANN and CFX models were measured by laboratory results and accuracy of each model was evaluated in flow prediction. Finally, velocity fields in some cross sections where laboratory findings are not available are calculated by ANN and compared with the results obtained from three dimensional numerical modeling.

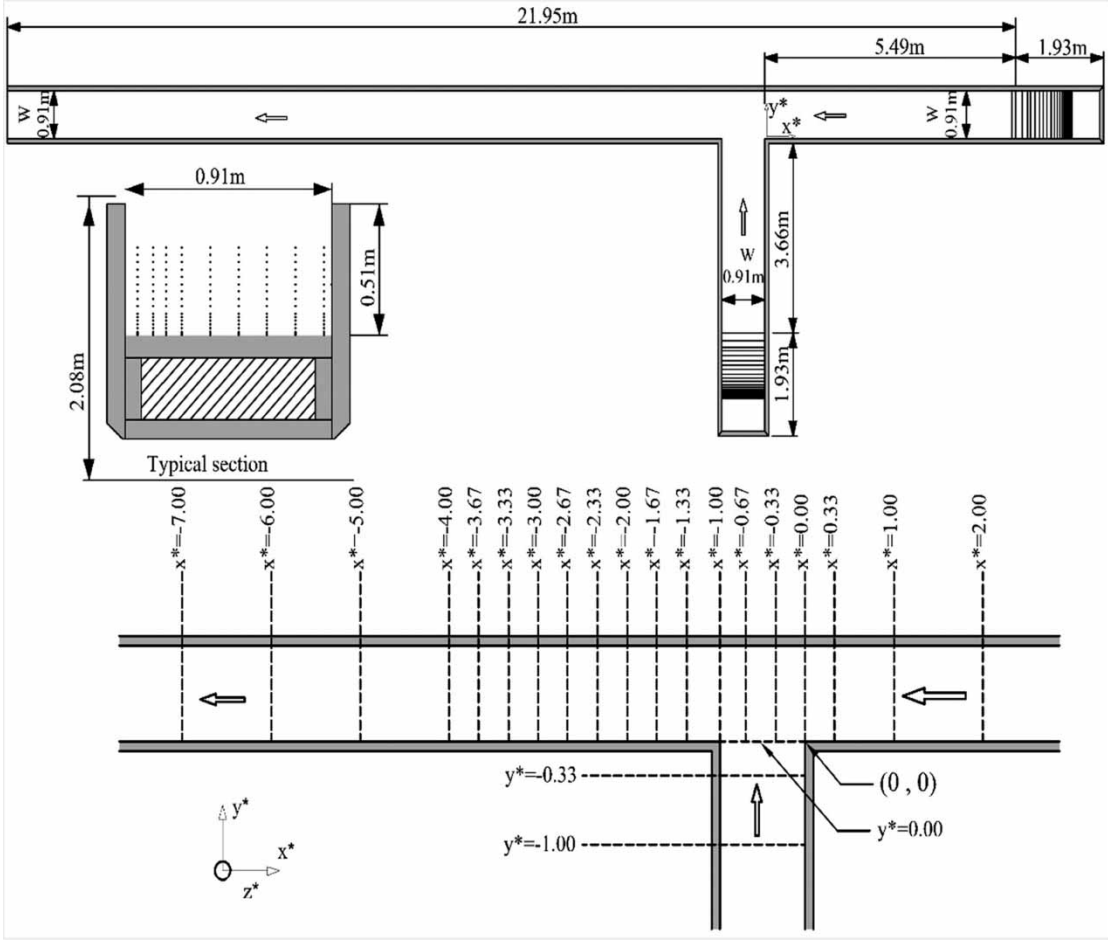

Figure 1. Experimental flume layout, Weber et al. (2001).

Table 1. Experimental flow conditions, Weber et al. (2001).

Q_m (m^3/s)	Q_b (m^3/s)	q*
0.014	0.156	0.083
0.042	0.127	0.250
0.071	0.099	0.417
0.099	0.071	0.583
0.127	0.042	0.750
0.156	0.014	0.917

2. Experimental model

In the present study, the laboratory results of Weber et al. (2001) and Shumate and Weber (1998) were used for validating ANN and numerical modeling results. The experiments were performed in a 90 degree combining flow flume as shown in Figure 1. While the junction has two branches, the upstream branches straight and the lateral branch has a junction angle of 90 degree. Two head tanks were placed in the entrance of main channel and branch channel that supplied the required flow into channels. Main and tributary channels had the same width ($=0.91$ m) and lengths of 21.95 m and 3.66 m, respectively. The slope of both channels was horizontal. The defined coordinate system had positive x-axis in the main channel's upstream direction. The positive y-direction points to the main channel wall which stands opposite to the positive z-axis upward in the vertical direction. All lengths to channel width ($=0.91$) were nondimensionalized. The nondimensionalized coordinates are shown with x*, y* and z* that are equivalent to x/W, y/W and z/W. Also, the measured velocities were nondimensionalized by downstream average velocity, ($V_t = 0.628$ m/s), and u*, v* and w* are equivalent to u/V_t, v/V_t and w/V_t respectively. Upstream main channel flow and branch channel flow are indicated with Q_m and Q_b respectively. Flow ratio q* is the ratio of main channel's upstream flow to total outflow of main and branch channels from the end of the channel ($q^* = Q_m/(Q_m + Q_b)$). The flow velocity is measured in flow conditions indicated in Table 1 in the marked cross sections (see Figure 1). More details about experiments are found in Weber et al. (2001). It should be noted that in all stages of the study, CFX and ANN numerical modeling, defined nondimensional coordinate system (x*, y*, z*) and nondimensional velocities (u*, v*, w*) were applied.

3. Methods

Initially, through ANSYS-CFX software, a three dimensional model was made and was compared with laboratory results. Then, through a genetic algorithm, an ANN was optimized in each layer for number of the hidden layer neurons. Using a part of laboratory data, ANN model was trained and tested with the other part. After evaluating ANN and CFX modeling error accuracy, under conditions in which no laboratory data are available, the results of ANN model were compared with those of CFX numerical simulation.

3.1. Model performance

The performance of an ANN is determined by comparing the predicted and observed outputs. There are several methods to quantify the difference between predicted and observed data, one of the most common of which is Mean Square Error (MSE) that defined as average of squares of the errors. In this study, model performance in ANN training process and GA objective function is calculated with MSE (Equation 1).

$$\mathrm{MSE} = \frac{1}{N}\sum_{i=1}^{N}(Y_{i_{observed}} - Y_{i_{estimated}})^2 \quad (1)$$

where N is the number of output and Y_i the velocity along x*. To analyze the accuracy of ANN in train and test data, MSE was computed separately.

To evaluate the accuracy of ANN model, Root Mean Square Error (RMSE), Mean Absolute Error (MAE), coefficient of determination (R^2), coefficient of efficiency (E_j), percent Standard Error Prediction (%SEP), Average Relative Variance (ARV), and average absolute deviation (%δ) were used. The advantage of RMSE and MAE models in evaluating the model error is that both use the same unit of variables. R^2 provides a measure of how well the observed outcomes are replicated by the model. The coefficient of efficiency by using $j=2$ (E_2) has been extremely used to evaluate the model accuracy (Leavesley, Lichty, Troutman, & Saindon, 1983; Wilcox, Rawls, Brakensiek, & Wight, 1990). If $E_2 = 1$, then ANN model has the perfect match to observed data, If it equals 0, then it indicates that the ability of ANN model in predicting longitudinal velocity is similar to average of observed data and if the value of E_2 is less than 1, the average of the observed data has higher accuracy than the ANN model (Nash & Sutcliffe, 1970). Due to squaring the difference terms in E_2, the high values of coefficient of efficiency were obtained (Willmott et al., 1985). In order to obtain the appropriate weighting of errors and decrease the effect of squared terms, the modified coefficient of efficiency by using $j=1$ (E_1) were used (Legates & McCabe, 1999). One of the significant advantages of %SEP and %δ is their nondimensionality which makes it possible to compare different models regardless of their dimension and size (Pulido-Calvo & Portela, 2007).

$$\mathrm{RMSE} = \sqrt{\mathrm{MSE}} \quad (2)$$

$$\mathrm{MAE} = \frac{1}{N}\sum_{i=1}^{N}|Y_{i_{estimate}} - Y_{i_{observed}}| \quad (3)$$

$$R^2 = \left[\frac{\sum_{i=1}^{n} (Y_{i_{observed}} - \overline{Y}_{observed})(Y_{i_{estimated}} - \overline{Y}_{estimated})}{\sqrt{\sum_{i=1}^{n} (Y_{i_{observed}} - \overline{Y}_{observed})^2 \sum_{i=1}^{n} (Y_{i_{estimated}} - \overline{Y}_{estimated})^2}} \right]^2 \quad (4)$$

$$E_j = 1 - \frac{\sum_{i=1}^{N} |Y_{i_{observed}} - Y_{i_{estimated}}|^j}{\sum_{i=1}^{N} |Y_{i_{observed}} - \overline{Y}_{observed}|^j} \quad (5)$$

$$ARV = \frac{\sum_{i=1}^{N} |Y_{i_{observed}} - Y_{i_{estimated}}|^2}{\sum_{i=1}^{N} |Y_{i_{observed}} - \overline{Y}_{observed}|^2} = 1 - E_2 \quad (6)$$

$$SEP = \frac{100}{\overline{Y}_{observed}} \times RMSE \quad (7)$$

$$\delta = \frac{\sum_{i=1}^{N} |Y_{i_{estimate}} - Y_{i_{observed}}|}{\sum_{i=1}^{N} Y_{i_{estimate}}} \times 100 \quad (8)$$

In these equations, $\overline{Y}_{observed}$ and $\overline{Y}_{estimated}$ are the average of the observed and estimated velocity along x* direction respectively.

3.2. Numerical model

The three dimensional numerical modelling is performed by commercial Ansys-CFX software package, which solves the three-dimensional fundamental flow equations. The vital equations for fluid motion in the whole domain are: (1) the Eulerian approach's continuity equation for the incompressible fluid and (2) the three Reynolds-Averaged Navier-Stokes (RANS) momentum equations for the incompressible turbulent fluid. Solving these equations require a turbulence model to set the Reynolds stresses. In this study, k-ω turbulence model (Wilcox, 1998) was used in which two transport equations are solved, one for the turbulent kinetic energy, k, and the other one for the turbulent frequency, ω.

To assess the accuracy of different turbulence models, RNG k-ϵ, k-ϵ and k-ω models were compared with the experimental results in same meshing (Table 2). The results indicate that RNG k-ϵ and k-ω models give more agreeable results than k-ϵ model. Although the accuracy of RNG k-ϵ and k-ω models is much close to each other, in some standard error measures like RMSE, MAE and R^2, k-ω was more reliable than RNG k-ϵ. Also, this model is used by various authors, Huang et al. (2002) and Shakibainia, Tabatabai, and Zarrati (2010) for simulations of flow in open channel junctions.

At the inlet, uniform velocity and water depth h are specified, turbulent intensity sets 5% (Bonakdari, Larrarte, & Bardiaux, 2007) and sufficient length is provided upstream of the junction to get a fully developed velocity profile. A length (10 m) is provided upstream of each inlet branch in order to obtain a fully developed turbulent flow when reaching the junction.

At the outlet, pressure is specified at the cell face center, while Cartesian velocity components and turbulence quantities are extrapolated from the interior using a second-order extrapolation. For the pressure correction equation, the pressure increment is set to zero at the outlet, as the pressure should not change during the solution. The rigid walls were set to smooth with no slip condition because it was considered appropriate for a laboratory flume. In the near wall area, Launder and Spalding (1974) method of standard wall function was used; that is, the velocity components are equal to zero in the walls. The free surface location is determined by the Volume of Fluid (VOF) method. The VOF technique, as described in Hirt and Nichols (1981), has been incorporated into the solution of the Navier–Stokes equations in order to take into account the free surface effects on the Reynolds stresses and, thus, velocity distribution in the cross section.

To find the best gridding, three mesh states, coarser mesh, mediocre mesh and finer mesh were used with 340526, 994652, and 2876399 elements respectively. The results of comparisons this three CFX models with

Table 2. Performance of CFX model in various turbulence models.

Turbulence	RMSE	MAE	R^2	%SEP	E_1	E_2	ARV	%δ
k-ϵ	0.233	0.201	0.487	− 44.798	− 1.356	− 7.989	8.989	− 32.922
RNG k-ϵ	0.187	0.145	0.595	− 23.791	− 0.019	− 0.150	1.15	− 16.060
k-ω	0.182	0.138	0.579	− 25.717	− 0.153	− 0.481	1.481	− 17.409

Table 3. Performance of CFX model in various mesh size.

Mesh	RMSE	MAE	R^2	%SEP	E_1	E_2	ARV	%δ
Coarser	0.234	0.192	0.623	− 49.425	− 1.864	− 11.291	12.291	− 26.779
Mediocre	0.182	0.138	0.579	− 25.717	− 0.153	− 0.481	1.481	− 17.409
Finer	0.162	0.124	0.566	− 22.051	0.127	0.141	0.859	− 16.656

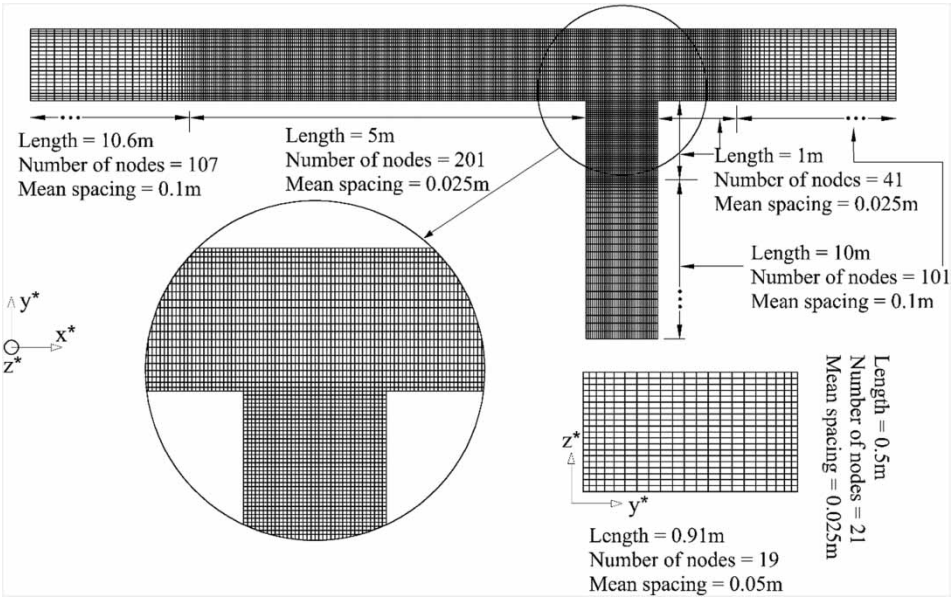

Figure 2. Details of computational mesh.

observed data in flow ratio of q* = 0.25 shown in Table 3. Comparison of coarser mesh state with that of mediocre mesh state indicates that the overall accuracy of the model has increased because RMSE value has decreased from 0.23 to 0.18 and %δ value has decreased from -27.66 to -17.40. On the contrary, the comparison of the mediocre mesh modeling results with those of finer mesh modeling indicates that RMSE error has decreased from 0.182 to 0.162 and %δ error has reduced from -17.40 to -16.65 indicating that reducing the mesh size has no significant effect on improving the results. In this study mediocre mesh modelling with 9,94,652 elements and 9,31,307 nodes were used.

A smaller mesh size was used around the confluence and a larger mesh size was used for upper and lower parts as shown in Figure 2. The numerical solution was terminated so that normalized residual would reach 10^{-6} for governing equations.

3.3. *Prediction using ANN*

In the first section, ANN model has been studied and then to optimize neural network structure, a modified genetic algorithm was introduced in the second section.

3.3.1. *Artificial neural network*

The flexible structure of ANN provides the capacity to make complex and nonlinear models between input and output. The capacity to estimate the correct results using input is based on training and learning processes. Training the neural networks means acquiring network weights (w). Also, various ANN are classified based on the methods of acquiring weights and transfer functions. One of the most applicable neural networks is Multi-Layer Perceptron (MLP). A feed forward MLP consists of an input layer or one or more hidden output layers. Every layer comprises a number of neurons. Neurons number in input layers is the same as the number of inputs and outputs of the given issue, respectively. In this study, four pieces of data were considered as input and one piece of data was considered as output. The inputs are nondimensional coordinates (x*, y* and z*) and flow ratio (q*), and target is nondimensional longitudinal velocity in x direction (u*). In the neural networks made for hidden-layer and output neurons, sigmoid and linear activation function are used, respectively. An f(x) function is of sigmoid type if it is bounded and is increased by increasing x value (Smith, 1993). However, diverse functions can be regarded as sigmoid function. In the present study, hyperbolic tangent was used in hidden layers as activation function. To train ANN, Levenberg-Marquardt method was applied (Guven & Kisi, 2011; More, 1978). In this method, back-propagation algorithm is used to find the weights and bias of neural network. It is one of the most useful algorithms in MLP neural network (Azamathulla & Ghani, 2011; Goh, 1995). This algorithm quantifies the difference between the outputs observed in laboratory studies and outputs of ANN model by determining weights and bias with high velocity.

To model the neural networks, the laboratory results obtained in flow ratio 0.083, 0.583 and 0.917, totally comprising 7348 pieces of data, are used. These data are divided into three parts: training, testing and validation. Data are randomly classified as 5142 (70%) into training data, 1103 (15%) into testing data and 1103 (15%) to validation data.

To investigate the potential of ANN model in predicting velocity profile in other flow ratios, in the next step, the

ANN model compare with the laboratory data in flow ratios $q^* = 0.25$ and $q^* = 0.75$ which virtually had no role in neural network train, validation and test was studied. Stop condition for ANN model is reaching 100 epochs.

So far, many parameters required were determined to define an MLP neural network like number and type of neurons in input and output layers, activation functions in hidden and output layers and training method. The number of hidden layers and the number of neurons in each layer are parameters important to define an MLP neural network. However, there is no definite principle to select these parameters and the number of layers and each layer's neurons should be tested to find the most optimized neural network (Bilhan et al., 2011; Melesse, Ahmad, McClain, Wang, & Lim, 2011). For example, if the required neural network can have 1–2 hidden layers and 1–20 neurons in each layer, we should test 420 states to find the optimized neural network, which is very difficult and time-consuming. In this study, the modified genetic algorithm was employed to identify the number of neurons in each of algorithm's layer.

3.3.2. *Genetic algorithm*

A common optimization algorithm in engineering sciences is genetic algorithm which was introduced by Holland (1975). The first step of the algorithm is creating a random initial population; then is creating a sequence of

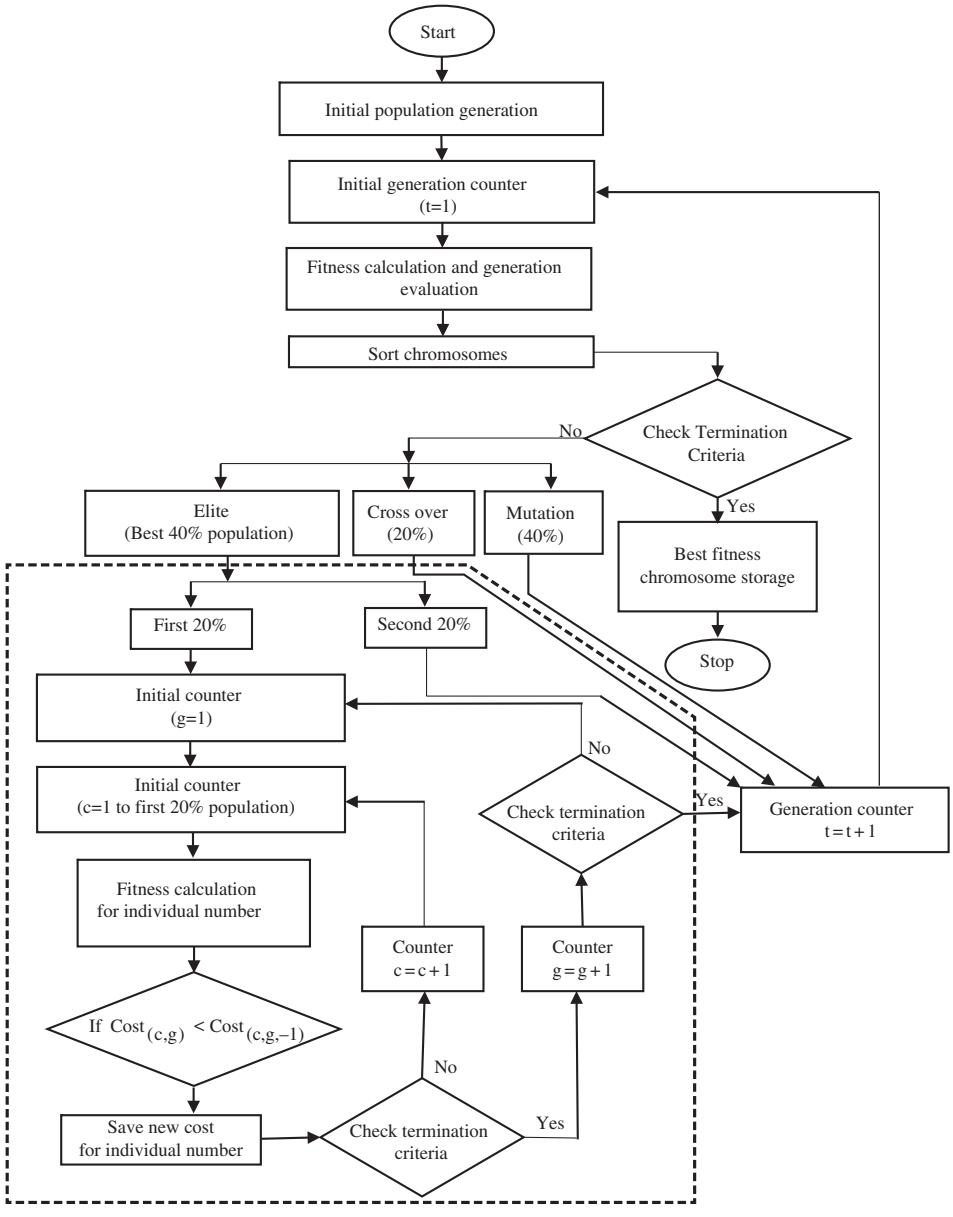

Figure 3. Flowchart of proposed GA.

Table 4. The MSE statistics of the two samples ANN models.

Runs	First ANN	Second ANN
1	0.0156	0.0098
2	0.0235	0.0129
3	0.1222	0.0234
4	0.0948	0.0345
5	0.0743	0.0143

new population, or generations. Each step consists of the algorithm's use of individuals in the current generation to produce the consequent generation. In creating a new generation, two steps are needed to be taken as shown in Figure 3, first, each member of the current population has to be scored by computing its fitness values; second, children should be reproduced from the current generation. To determine the individual population cost in genetic algorithm, the cost of every individual was calculated by Equation (9) in order to prevent the possible overtraining of ANN. Overtrain is a state in which there is a big difference between test and train data accuracy. A good ANN model is one in which test and train data accuracy are close to each other. To investigate the goodness of each chromosome in GA (ANN models with different structures), instead of using MSE_{test} or MSE_{train} separately, the sum of both coefficients is used. In GA model, a chromosome is considered to be superior in which the sum of its MSE_{test} and MSE_{train} is minimum (Equation 9). Also by giving different values to C_{test} and C_{train}, one can use MSE_{test} and MSE_{train} weighted sum. C_{test} and C_{train} parameters can be determined by trial and error method.

$$\cos t_i = C_{train} \times MSE_{i_{train}} + C_{test} \times MSE_{i_{test}} \quad (9)$$

C_{test} and C_{train} are coefficients that indicate the importance we give to the train and test data. They are determined experimentally in terms of neural network and data. In this study, they are given value 1. Children are reproduced via Elite, crossover and mutation. When the new population is created, it replaces the current population with the children so that creation of the next generation becomes possible. Meeting one of the stopping criteria leads in the stop of the algorithm.

Due to the random selection of neural network in selecting the test and train data from the present dataset, even when all parameters of an ANN like number of layers, neurons in each layer and activation function are retrained by ANN model, we do not obtain previous series of MSE; instead, we obtain a specific MSE in each training. For instance, in Table 4, two 4-layer neural networks (one input, two hidden and one output) are trained with the present data. In the first ANN in each hidden layer, 3 neurons are used and in the second ANN, 6 neurons are used in each hidden layer. Then, the produced neural networks are trained 5 times. Due to random selection of train and test data in each training, the MSEs obtained are not the same, Table 4 indicates that the second ANN provides better results than the first ANN. This feature of the neural network makes optimization algorithm used to optimize the neural networks is trapped by local minimums and produces incorrect responses. To solve this problem, it is necessary to make a little change in the elite section of creating the next generation, indicated in Figure 3 with dash line.

Elite children refer to individuals in the current generation that are identified as having the best fitness values. These individuals automatically pass to the subsequent generation. The changes made were intended to prevent elimination of good individuals in the transfer process to the next generation. By 40 times repetitions in the top 20% of the population, the best fitness value that each individual has gained in these repetitions is substituted for the fitness value of that individual. Thus, falling in a local minimum cannot make any changes in the top 20% of population and they only change when, due to mutation or crossover, an individual is produced with a fitness value better than that of the top 20% of the population after 40 repetitions. In the present model, having optimized the network with modified GA, the number of neurons in layers 2 and 3 was 9 in a 4-layer neural network. The performance of optimized ANN is shown in Table 5. In this table, closer the values of RMSE, MAE, %SEP, AVR and %δ get to 0 and closer the values of E_1, E_2, R^2 to 1, shown the model has higher accuracy. As seen from 5, as expected train data as compared to validation and test data has higher accuracy. The closeness of train, validation and test data indicates that ANN model does not trap in overtrain. Based on %SEP and %δ error in all data, one can conclude that on the whole optimized ANN model has %12.90 and %-9.45 error, respectively. This values indicating its agreeable accuracy in longitudinal velocity modelling (u*).

Table 5. Performance of optimized ANN model.

Data set	RMSE	MAE	R^2	%SEP	E_1	E_2	ARV	%δ
Train	0.086	0.064	0.963	– 12.652	0.833	0.963	0.036	– 9.349
Test	0.094	0.067	0.956	– 13.691	0.823	0.956	0.043	– 9.754
Validation	0.091	0.066	0.959	– 13.284	0.829	0.959	0.040	– 9.634
All data	0.088	0.064	0.962	– 12.908	0.831	0.962	0.038	– 9.453

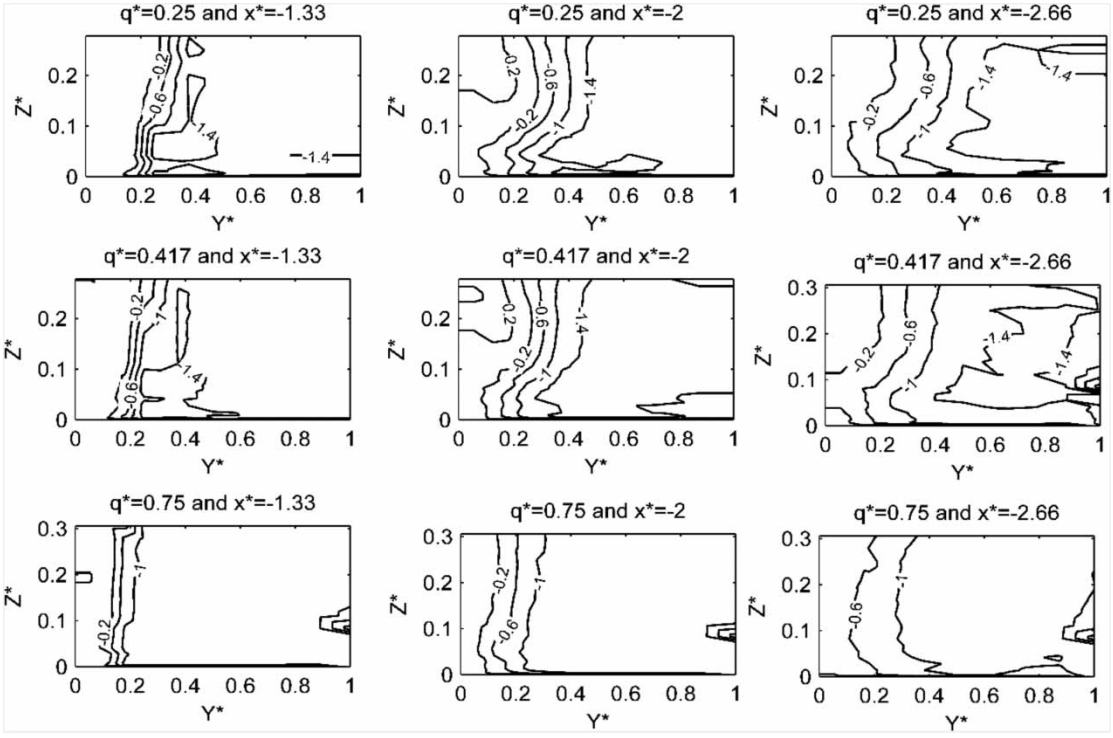

Figure 4. Contours of longitudinal velocity.

4. Results

4.1. Investigation of variation of longitudinal velocity

As mentioned, longitudinal velocity, u*, indicates nondimensionalized velocity along x. In Figure 4, the u*-velocity contours for x* = −1.33, −2 and −2.66 are shown in q* = 0.250, 0.417 and 0.750. Slightly after confluence in longitudinal walls of the channel, an area is created in whose boundaries velocity is decreased and in which recirculation occurs, indicated in Figure 4 with positive velocities, this region is called separation zone.

The comparison of Figure 4 in q* = 0.250, 0. 417 and 0.750 indicated that by increasing the flow in the main channel and increasing q* in a constant x* (e.g. x* = -2), the separation zone dimensions are decreased due to flow momentum decline in the branch channel owing to q* increase. On the other hand, when q* is low, due to high momentum of the branch flow, it is diverted to the downstream side of the main channel when it enters the main channel and two flows join each other. This increases the separation zone dimensions. Moreover, by moving from the channel floor to the surface of the water, the separation zone dimensions are increased and consequently recirculation and velocity are increased in the direction opposite to the flow. Another area that happens in the downstream junctions is constricted area that occurs in the right side of the sections (in y* between 0.5 and 1) (Figure 4). The more is the constriction of the flow, the higher is the flow velocity. The intensity of constriction is directly associated with separation zone width, and the constriction rate and flow velocity are increased by increasing the width of this area. Unlike open channels in which the highest velocity occurs near the free surface, in this area the maximum velocity occurs near the channel bed. However, by distancing the confluence, the velocity profile in the channel returns to normal state and the highest velocity happens in the flow surface.

4.2. Results of CFX

Longitudinal velocity distribution values obtained from the numerical model made by ANSYS-CFX software were compared with laboratory values in x* = -2 and -3 and in q* = 0.250 and 0.750 illustrated in Figure 5. In this figure, the horizontal axis indicates nondimensionalized values of the channel's width (y*) and the vertical axis shows nondimensionalized values along the water depth (z*). As it is indicated, the numerical and laboratory models were in good agreement and there were only differences between numerical and laboratory values in some points near the wall on y* = 0. Figure 5 shows that the velocity value in the opposite direction of the flow even in x* = −2, which is located in the middle of the separation zone, are very small compared to the longitudinal velocity and this value is decreased by moving from x* = −2 to x* = −3. In fact, by distancing the flow confluence, it tries to

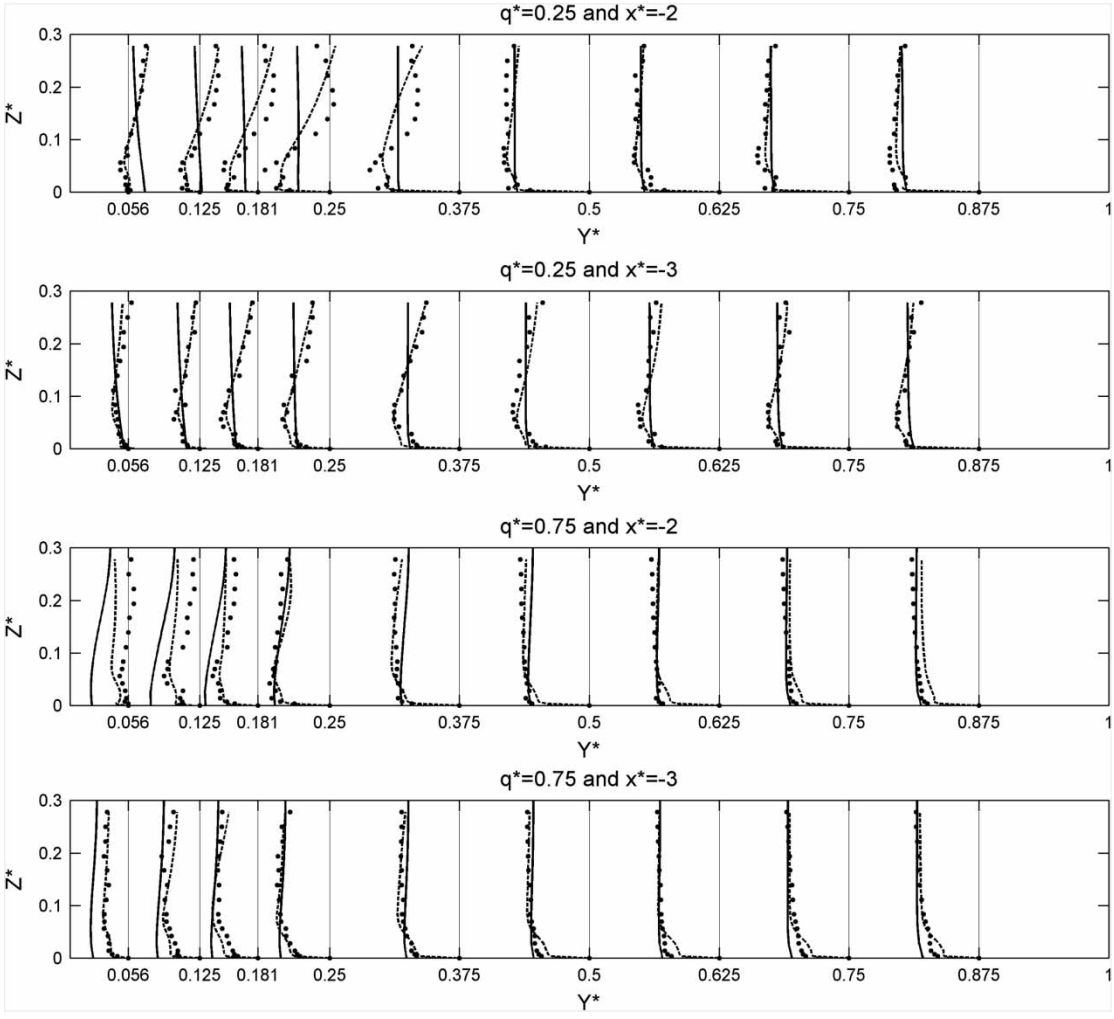

Figure 5. Longitudinal velocity profiles in measurements (. . .) and 3D CFX ( ) and ANN (—) simulations.

return to the typical state of flow in open channel, but this recovery is very slow and occurs in a length 3 times more than the confluence point to $x^* = -2$ point (Dursun et al., 2012; Huang et al., 2002). Contours a, b, c and d in Figure 6 indicate the error of the results obtained from CFX model compared to laboratory findings. Given these contours in $q^* = 0.250$ and $x^* = -2$ and -3, the typical error is about 7%, which is increased to 20% locally and 30% in very small areas. The higher accuracy of numerical modeling in $q^* = 0.750$ than in $q^* = 0.250$ is because of recirculation zone reduction in high q* owing to weakening of inflow from branch channel to main channel and decline of flow displacement in the main channel.

4.3. *Results of ANN*

As cited before, ANN model used in this study is a four-layer ANN that consists of an input layer, an output layer and two hidden layers; the input layer includes nondimensionalized coordinate of the given point (z*, y*, x*) and flow ratio in flow conditions (q*). The input layer has totally four inputs and output layer has one output, which is the longitudinal velocity of flow (u*). After optimization of ANN model by modified genetic algorithm, the number of neurons existing in the two hidden layers was 9. The characteristics of modified genetic algorithm are presented in Figure 3, laboratory data in $q^* = 0.083$, 0.583 and 0.917 for ANN modeling were used and the input data were totally 7348. Since the input values of neural network (x*, y*, z* and q*) were nondimensionalized, the obtained neural network can be used for every open channel junction with desirable dimensions and flow ratios. Therefore, the Equation (10) was extracted in this study to determine the longitudinal velocities (u*) in every open channel junction for x*, y*, z* and q* inputs of trained ANN, where B_1, B_2 and B_3 stand as bias values for the first, second and third layers and W_1, W_2 and W_3 are weight values for first,

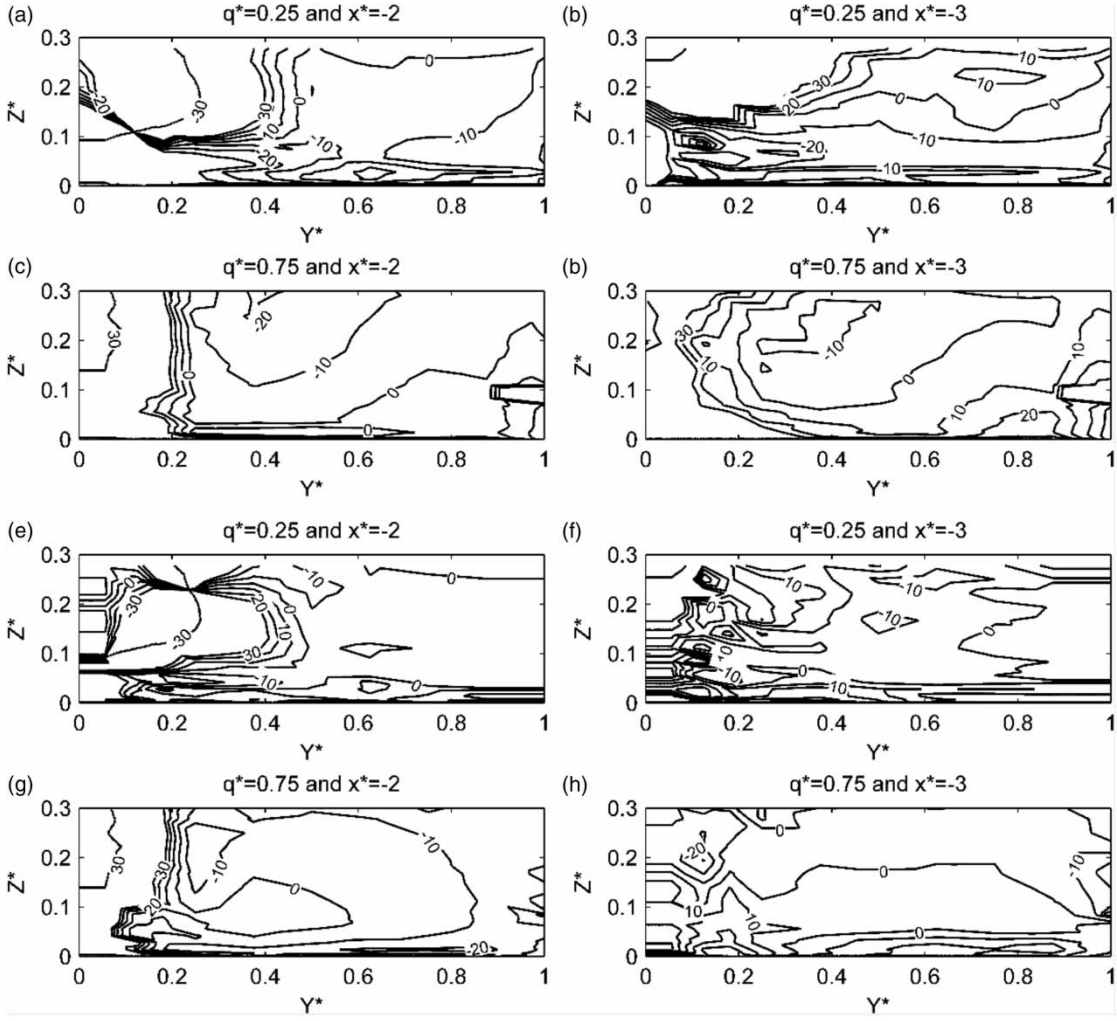

Figure 6. Error of the longitudinal velocity predicted (u^*_{calc}) by CFX model (a,b,c,d) and ANN model (e,f,g,h) compared to experimental data (u^*_{exp}) that given as (u^*_{calc}-u^*_{exp})/ u^*_{exp} in %.

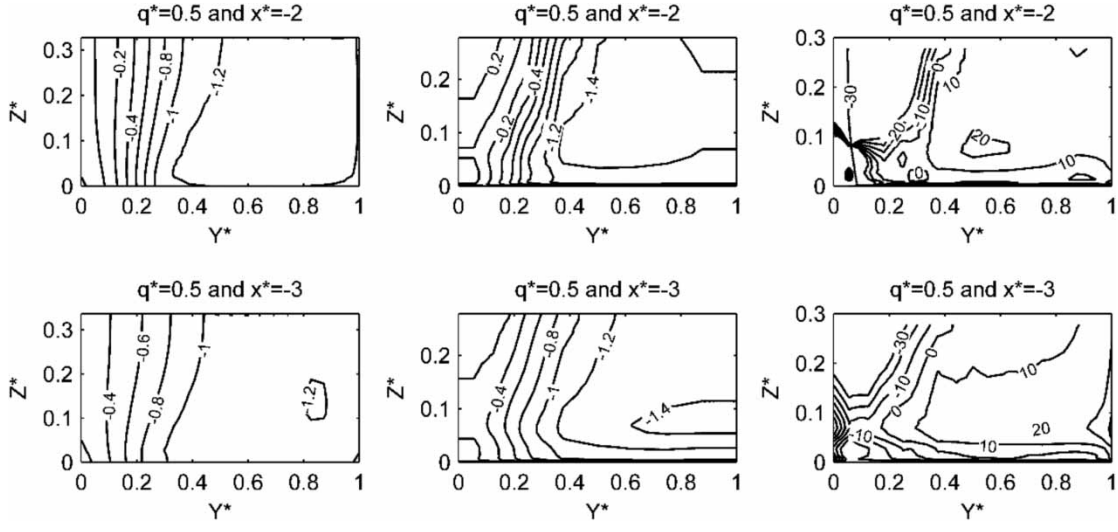

Figure 7. Longitudinal velocity profile where we don't have experimental data in CFX simulation (the left column) and ANN model (the middel column) and their deviation that given as (u*cfx-u*ann)/ u*cfx in % (the right column)

second and third layers, respectively, which are shown in Equations (11) to (16). Matrix I shows the inputs of the problem presented in Equation (17). Also, F_1, F_2 and F_3 are activation functions used in ANN model. As shown in Equations (18) and (19), F_1 and F_2 are sigmoid functions and the F_{out} function in the present model is a linear function. In Figure 5, the values of longitudinal velocities (u*) obtained from ANN are compared with those obtained from laboratory results. The findings of the error contours in this figure indicate that despite not using laboratory results for q* = 0.25 and 0.75 in the train and test of the neural networks, the results of ANN model in this q* are compatible with laboratory results. This shows that this model can be used to acquire the profiles of longitudinal velocities in every flow ratio (q*). The error contours of e, f, g and h in Figure 6, which indicate the error resulting from ANN model compared to laboratory results, show that the typical error is around 5% in both q* = 0.250 and q* = 0.750, and the local error in x* = −2, which has a remarkable recirculation, is 30% and in x* = −3 is 20% because it is slightly distanced from the separation zone. Based on the comparison of the results of CFX and ANN shown in Figure 5 and the error values of these models with those of laboratory model presented in Figure 6, it is obvious that ANN is more accurate than CFX in modelling the velocity field in open channel junction zone, which is more noticeable in recirculation zone that is the major deficiency of CFD models in flow modeling in confluence zone.

$$u^* = F_{out}(F_2(F_1(I_{(1\times4)} \times W_{1_{(4\times9)}} + B_{1_{(1\times9)}}) \times W_{2_{(9\times9)}} + B_{2_{(1\times9)}}) \times W_{3_{(9\times1)}} + B_{3_{(1\times1)}}) \quad (10)$$

$$B_{1_{(1\times9)}} = [-2.3579 \quad 2.9795 \quad 26.9251 \quad -5.3245 \quad 1.3823 \quad 0.1175 \quad -2.0678 \quad 0.8528 \quad 5.3748] \quad (11)$$

$$B_{2_{(1\times9)}} = [-11.3620 \quad 3.9181 \quad -1.9545 \quad -1.8640 \quad 9.8659 \quad 1.9582 \quad -0.8594 \quad 2.4295 \quad 0.6613] \quad (12)$$

$$B_{3_{(1\times1)}} = [6.1646] \quad (13)$$

$$W_{1_{(4\times9)}} = \begin{bmatrix} 7.6695 & -1.7634 & -0.0668 & 21.3580 & -0.6429 \\ 0.0291 & -0.0141 & -0.0136 & -0.1525 & -0.3292 \\ 0.2153 & -0.2092 & 25.8747 & 0.1791 & 0.7555 \\ 0.1834 & 2.9233 & -0.0213 & 0.2169 & 0.2895 \end{bmatrix}$$

$$\begin{bmatrix} -2.7991 & -0.6072 & 0.5022 & 0.4061 \\ -0.3027 & -4.3405 & -0.5962 & 0.1870 \\ -0.1116 & 0.8210 & -0.1163 & 6.9672 \\ 0.0555 & -0.3815 & -1.8503 & -0.1503 \end{bmatrix} \quad (14)$$

$$W_{2_{(9\times9)}} = \begin{bmatrix} -0.9104 & 1.2005 & 0.0835 & -0.1722 & -0.6964 \\ -0.1734 & 0.1189 & -0.0424 & 0.0362 & 0.0660 \\ -3.9389 & -1.9558 & 0.6751 & 1.1518 & -10.3368 \\ -0.0619 & 0.0640 & 0.2884 & -0.1684 & -0.0726 \\ -1.5376 & -0.4020 & 0.1708 & 0.3452 & -0.7708 \\ -0.1672 & 0.4823 & 0.4216 & -0.1457 & 1.4878 \\ -0.7921 & 0.5462 & 0.4421 & 0.1852 & 0.6746 \\ 0.1593 & -0.0391 & 0.1520 & 0.1050 & -0.5545 \\ -14.6429 & -0.0519 & -0.0186 & 0.0106 & -0.4693 \end{bmatrix}$$

$$\begin{bmatrix} 0.0179 & -0.1343 & 1.0064 & 1.3996 \\ -0.0033 & -0.0333 & 0.2678 & 0.0166 \\ -0.9751 & 0.8998 & -0.9374 & 0.6126 \\ 0.0373 & -0.6531 & 0.0336 & 0.5911 \\ -0.2888 & 0.0275 & -0.2570 & 0.0704 \\ -0.0677 & 0.6639 & -0.4353 & 0.4832 \\ -0.2234 & 0.7911 & 0.6830 & -1.2219 \\ -0.1418 & 0.0273 & -0.2191 & 0.3587 \\ -0.0030 & -0.0376 & -0.0784 & 0.1619 \end{bmatrix} \quad (15)$$

$$W_{3_{(9\times1)}} = [2.3321 \quad -7.0601 \quad -13.1806 \quad -16.4147 \quad 0.3578 \quad -29.1941 \quad 3.3368 \quad 5.2391 \quad 1.6925]^T \quad (16)$$

$$I_{(1\times4)} = [x* \quad y* \quad z* \quad q*] \quad (17)$$

$$F_1(x) = F_2(x) = \tanh(x) \quad (18)$$

$$F_{out}(x) = x \quad (19)$$

4.4. *Comparison of results CFX and ANN*

The comparison of Figures 5 and 6 shows that the areas out of the recirculation zone of ANN and CFX models have rather the same accuracy, but the main difference is the accuracy of these models in obtaining longitudinal velocities (u*) in inner areas of recirculation in which ANN model is more successful than CFX model. The main purpose of CFX numerical modeling and ANN training and their validation with laboratory model is analyzing the reliability of them in obtaining longitudinal velocities in conditions where there is no laboratory studies. That is why in Figure 7 where no measurement has been done in laboratory studies for q* = 0.500 (Shumate & Weber, 1998; Weber et al., 2001), the contours of longitudinal velocities (u*) are designed by numerical CFX model (left column) and trained by ANN model or by Equation (8) (middle column). If the deviation between the results of CFX and ANN is expressed by percentage (right column), it can be seen that both models have good agreement and the typical error in x* = -2 is approximately 15% and in x* = -3 around 10%, which is indicative of the reliability of both CFX and ANN models and their high accuracy in flow modeling in open channel junction.

5. Conclusion

In this study, GA-ANN, three dimensional numerical model and laboratory data were used to analyze and predict the longitudinal velocity in 90 degree open channel junction. First, the genetic algorithm was modified to be appropriate for optimization of the random structure of neural network and ANN model was optimized to predict the longitudinal velocity in different sections of an open channel junction in various flow ratios. To train the neural network, Levenberg-Marquardt method was applied. Then, ANN model was compared with laboratory results and its error was analyzed. The findings indicated the high accuracy of ANN model to predict the velocity profiles in junctions even in complex areas of flow like separation

zone. Finally, the equation extracted from the produced neural network was presented for predicting the flow velocity that can be used for every 90 degree open channel junction with every flow ratio. A three dimensional two-phase flow (water + air) numerical model was made by ANSYS-CFX software and the results obtained to predict the longitudinal velocities were compared with laboratory findings. The findings indicated a good accuracy for CFX model. Moreover, the results of ANN and CFX models in $q^* = 0.500$ were compared and the results showed good agreement between the results obtained from both models. Finally, by comparing the results of CFX and ANN models, it can be argued that, except in recirculation zone areas where ANN model produces better results, the accuracy in other flow areas of both models are almost the same.

References

Asadi, S., Shahrabi, J., Abbaszadeh, P., & Tabanmehr, S. (2013). A new hybrid artificial neural networks for rainfall-runoff process modeling. *Neurocomputing*, *121*, 470–480.

Azamathulla, H. M., & Ghani, A. A. (2011). Genetic programming for predicting longitudinal dispersion coefficients in streams. *Water Resources Management*, *25*(6), 1537–1544.

Best, J. L., & Reid, I. (1984). Separation zone at open-channel junctions. *Journal of Hydraulic Engineering – ASCE*, *110*(11), 1588–1594.

Bilhan, O., Emiroglu, M. E., & Kisi, O. (2011). Use of artificial neural networks for prediction of discharge coefficient of triangular labyrinth side weir in curved channels. *Advances in Engineering Software*, *42*(4), 208–214.

Biron, P., Best, J. L., & Roy, A. G. (1996). Effects of bed discordance on flow dynamics at open channel confluences. *Journal of Hydraulic Engineering*, *122*(12), 676–682.

Bonakdari, H., Larrarte, F., & Bardiaux, J. (2007). Experimental and computational study of velocity fields in narrow or compound section sewers. *Water Practice & Technology*, *2*(2), 1–8.

Bonakdari, H., Lipeme-Kouyi, G., & Wang, X. (2011, May 22–26). *Experimental validation of CFD modeling of multiphase flow trough open channel confluence*. World Environmental and Water Resources Congress 2011: Bearing Knowledge for Sustainability, Palm Springs, CA, pp. 2176–2183.

Bradbrook, K. F., Biron, P. M., Lane, S. N., Richards, K. S., & Roy, A. G. (1998). Investigation of controls on secondary circulation in a simple confluence geometry using a three-dimensional numerical model. *Hydrological Processes*, *12*(8), 1371–1396.

Bradbrook, K. F., Lane, S. N., & Richards, K. S. (2000a). Numerical simulation of three-dimensional, time-averaged flow structure at river channel confluences. *Water Resources Research*, *36*(9), 2731–2746.

Bradbrook, K. F., Lane, S. N., Richards, K. S., Biron, P. M., & Ag, R. (2000b). Large Eddy Simulation of periodic flow characteristics at river channel confluences. *Journal of Hydraulic Research*, *38*(3), 207–215.

Chau, K. W., Wu, C. L., & Li, Y. S. (2005). Comparison of several flood forecasting models in Yangtze River. *Journal of Hydrologic Engineering*, *10*(6), 485–491.

Chen, W., & Chau, K. W. (2006). Intelligent manipulation and calibration of parameters for hydrological models. *International Journal of Environment and Pollution*, *28*(3–4), 432–447.

Cheng, C. T., Lin, J. Y., Sun, Y. G., & Chau, K. (2005, August 27–29). *Long-term prediction of discharges in Manwan Hydropower using adaptive-network-based fuzzy inference systems models*. First International Conference on Natural Computation, ICNC 2005, Changsha, pp. 1152–1161.

Chung-Chieh, H., Wen-Jung, L., & Cheng-Hsi, C. (1998). Subcritical open-channel junction flow. *Journal of Hydraulic Engineering*, *124*(8), 847–855.

Cobaner, M. (2011). Evapotranspiration estimation by two different neuro-fuzzy inference systems. *Journal of Hydrology*, *398*(3–4), 292–302.

Donmez, S. (2011). Using artificial neural networks for prediction of alternate depth shaped on rectangular channel in open channel flow. *Energy Education Science and Technology Part A: Energy Science and Research*, *28*(1), 339–348.

Dursun, O. F., Kaya, N., & Firat, M. (2012). Estimating discharge coefficient of semi-elliptical side weir using ANFIS. *Journal of Hydrology*, *426–427*, 55–62.

Ebtehaj, I., & Bonakdari, H. (2013). Evaluation of sediment transport in sewer using artificial neural network. *Engineering Applications of Computational Fluid Mechanics*, *7*(3), 382–392.

Firat, M., & Gungor, M. (2008). Hydrological time-series modelling using an adaptive neuro-fuzzy inference system. *Hydrological Processes*, *22*(13), 2122–2132.

Goh, A. T. C. (1995). Back-propagation neural networks for modeling complex systems. *Artificial Intelligence in Engineering*, *9*(3), 143–151.

Grace, J. L., & Priest, M. S. (1958). *Division of flow in open channel junctions*. Auburn, AL: Engineering Experiment Station, Alabama Polytechnic Institute.

Guven, A., & Kisi, O. (2011). Estimation of Suspended Sediment Yield in Natural Rivers Using Machine-coded Linear Genetic Programming. *Water Resources Management*, *25*(2), 691–704.

Hager, W. H. (1987). Discussion of "Separation Zone at Open-Channel Junctions" by James L. Best and Ian Reid (November, 1984). *Journal of Hydraulic Engineering*, *113*(4), 539–543.

Hirt, C. W., & Nichols, B. D. (1981). Volume of fluid (VOF) method for the dynamics of free boundaries. *Journal of Computational Physics*, *39*(1), 201–225.

Holland, J. (1975). Genetic Algorithms, computer programs that evolve in ways that even their creators do not fully understand. *Scientific American*, (267), 66–72.

Huang, J., Weber, L. J., & Lai, Y. G. (2002). Three-dimensional numerical study of flows in open-channel junctions. *Journal of Hydraulic Engineering*, *128*(3), 268–280.

Kisi, O., & Ozturk, O. (2007). Adaptive neurofuzzy computing technique for evapotranspiration estimation. *Journal of Irrigation and Drainage Engineering*, *133*(4), 368–379.

Launder, BE., & Spalding, D. B. (1974). The numerical computation of turbulent flows. *Computer Methods in Applied Mechanics and Engineering*, *3*(2), 269–289.

Leavesley, G. H., Lichty, R., Troutman, B., & Saindon, L. (1983). *Precipitation-runoff modeling system: User's manual*. Colorado, CO: US Geological Survey.

Legates, D. R., & McCabe, Jr G. J. (1999). Evaluating the use of 'goodness-of-fit' measures in hydrologic and hydroclimatic model validation. *Water Resources Research*, *35*(1), 233–241.

Lin, J. D., & Soong, H. K. (1979). Junction losses in open channel flows. *Water Resources Research*, *15*(2), 414–418.

Melesse, A. M., Ahmad, S., McClain, M. E., Wang, X., & Lim, Y. H. (2011). Suspended sediment load prediction of river

systems: an artificial neural network approach. *Agricultural Water Management*, *98*(5), 855–866.

More, J. J. (1978). The Levenberg-Marquardt algorithm: Implementation and theory, In G. A. Watson (Ed.), *Lecture Notes in Mathematics 630* (pp. 105–116). New York: Springer-Verlag.

Muttil, N., & Chau, K. W. (2006). Neural network and genetic programming for modelling coastal algal blooms. *International Journal of Environment and Pollution*, *28*(3–4), 223–238.

Muzzammil, M. (2010). ANFIS approach to the scour depth prediction at a bridge abutment. *Journal of Hydroinformatics*, *12*(4), 474–485.

Nash, J. E., & Sutcliffe, J. V. (1970). River flow forecasting through conceptual models part I - A discussion of principles. *Journal of Hydrology*, *10*(3), 282–290.

Neary, V. S., & Sotiropoulos, F. (1996). Numerical investigation of laminar flows through 90-degree diversions of rectangular cross-section. *Computers and Fluids*, *25*(2), 95–118.

Pulido-Calvo, I., & Gutierrez-Estrada, J. C. (2009). Improved irrigation water demand forecasting using a soft-computing hybrid model. *Biosystems Engineering*, *102*(2), 202–218.

Pulido-Calvo, I., & Portela, M. M. (2007). Application of neural approaches to one-step daily flow forecasting in Portuguese watersheds. *Journal of Hydrology*, *332*(1–2), 1–15.

Ramamurthy, A. S., Carballada, L. B., & Tran, D. M. (1988, December 12). Combining open channel flow at right angled junctions. *Journal of Hydraulic Engineering*, *114*, 1449–1460.

Shakibainia, A., Tabatabai, M. R. M., & Zarrati, A. R. (2010). Three-dimensional numerical study of flow structure in channel confluences. *Canadian Journal of Civil Engineering*, *37*(5), 772–781.

Shamloo, H., & Pirzadeh, B. (2008). Investigation of characteristics of separation zones in T-junctions. *WSEAS Transactions on Mathematics*, *7*(5), 303–312.

Shumate, ED., & Weber, L. J. (1998, August 3–7). *Experimental description of combining flows at an open channel junction*. Proceedings of the 1998 International Water Resources Engineering Conference. Part 2 (of 2). ASCE, Reston, VA, pp. 1679–1684.

Smith, M. (1993). *Neural networks for statistical modeling*. New York, NY: Thomson Learning.

Taormina, R., Chau, K. W., & Sethi, R. (2012). Artificial neural network simulation of hourly groundwater levels in a coastal aquifer system of the Venice lagoon. *Engineering Applications of Artificial Intelligence*, *25*(8), 1670–1676.

Taylor, EH. (1944). Flow characteristics at rectangular open-channel junctions. *Transactions of the American Society of Civil Engineers*, *109*(1), 893–902.

Tiwari, M. K., & Adamowski, J. (2013). Urban water demand forecasting and uncertainty assessment using ensemble wavelet-bootstrap-neural network models. *Water Resources Research*, *49*(10), 6486–6507.

Van Maanen, B., Coco, G., Bryan, K. R., & Ruessink, B. G. (2010). The use of artificial neural networks to analyze and predict alongshore sediment transport. *Nonlinear Processes in Geophysics*, *17*(5), 395–404.

Wang, X., & Cheng, L. (2000). Three-dimensional simulation of a side discharge into a cross channel flow. *The Computational Techniques and Applications Conference*, *29*(4), 415–433.

Webber, N. B., & Greated, C. (1966). An investigation of flow behaviour at the junction of rectangular channels. *ICE Proceedings*, *34*(3), 321–334.

Weber, L. J., Schumate, E. D., Mawer, N. (2001). Experiments on flow at a 90° open-channel junction. *Journal of Hydraulic Engineering*, *127*(5), 340–350.

Wilcox, B. P., Rawls, W. J., Brakensiek, D. L., & Wight, J. R. (1990). Predicting runoff from rangeland catchments: a comparison of two models. *Water Resources Research*, *26*(10), 2401–2410.

Wilcox, D. C. (1998). *Turbulence modeling for CFD* (2nd ed.). La Canada Flintridge, CA: D C W Industries Inc.

Willmott, C. J., Ackleson, S. G., Davis, R. E., Feddema, J. J., Klink, K. M., Legates, D. R., O'Donnell, J., & Rowe, C. M. (1985). Statistics for the evaluation and comparison of models. *Journal of Geophysical Research: Oceans (1978-2012)*, *90*(C5), 8995–9005.

Wu, C. L., Chau, K. W., & Li, Y. S. (2009). Predicting monthly streamflow using data-driven models coupled with data-preprocessing techniques. *Water Resources Research*, *45*(8), 1–23.

Yurtseven, I., & Zengin, M. (2013). Neural network modelling of rainfall interception in four different forest stands. *Annals of Forest Research*, *56*(2), 351–362.

Zhao, C. H., Zhu, D. Z., & Rajaratnam, N. (2008). Computational and experimental study of surcharged flow at a 90° combining sewer junction. *Journal of Hydraulic Engineering*, *134*(6), 688–700.